arXiv:1604.08497v2 [cond-mat.mtrl-sci] 3 Jun 2016

Influence of halide composition on the structural, electronic and optical properties of mixed $CH_3NH_3Pb(I_{1-x}Br_x)_3$ perovskites with virtual crystal approximation method

Un-Gi Jong,[1] Chol-Jun Yu*,[1] Jin-Song Ri,[1] Nam-Hyok Kim,[2] and Guk-Chol Ri[2]

[1]*Department of Computational Materials Design, Faculty of Materials Science, and* [2]*Department of Theoretical Physics, Faculty of Physics, Kim Il Sung University, Ryongnam-Dong, Taesong District, Pyongyang, DPR Korea*

(Dated: June 6, 2016)

Abstract

Extensive studies undertaken recently have demonstrated promising capability of the hybrid halide perovskite $CH_3NH_3PbI_3$ in solar cells with high power conversion efficiency exceeding 20%. However, the existence of intrinsic and extrinsic instability in these materials remain a major challenge to commercialization. Mixing halides is expected to resolve this problem. Here we investigate the effect of chemical substitution on the structural, electronic and optical properties of mixed halide $CH_3NH_3Pb(I_{1-x}Br_x)_3$ perovskites using the virtual crystal approximation method within density functional theory. As the Br content x increases from 0.0 to 1.0, the lattice constant decreases in proportion to x with a function of $a(x) = 6.420 - 0.333x$ (Å), while the band gap and the exciton binding energy increase with a quadratic function of $E_g(x) = 1.542 + 0.374x + 0.185x^2$ (eV) and a linear function of $E_b(x) = 0.045 + 0.057x$ (eV) respectively. The photoabsorption coefficients are also calculated, showing blue-shift of the absorption onsets for higher Br contents. Based on the computational results and through the analysis of chemical bonding characteristics, we suggest that the best match between efficiency and stability can be achieved at x=0.2 in $CH_3NH_3Pb(I_{1-x}Br_x)_3$ perovskites.

PACS numbers: 88.40.H-; 71.35.-y; 78.20.Ci; 31.15.A-

* Corresponding author: ryongnam14@yahoo.com

I. INTRODUCTION

Perovskites based solar cells (PSCs) are affording a promise of bright future of solar energy utilization, with the fast rise of power conversion efficiency already exceeding 20% [1, 2], remarkably easy fabrication process [3–5], and moderately low cost and sufficient supply of raw materials [6, 7]. The key component for governing the PSC's performance is methylammonium lead tri-iodide perovskite ($CH_3NH_3PbI_3$ or $MAPbI_3$) that is used as charge carrier mediator as well as light absorber. Numerous studies undertaken for the past five years have proven that this material has ideal properties for solar cell applications such as optimal band gap around 1.5 eV [8], large absorption coefficients [9–11], weak exciton binding energy ($<$ 0.05 eV) [12, 13], high mobility of free charge carrier [14–17], and exceptionally large charge diffusion length over 100 μm [18]. However, it also turned out that $MAPbI_3$ suffers from the poor material stability, which represents a significant challenge on route to development of commercially viable PSCs, and yet a microscopic understanding of the degradation process remains debatable [19–21].

Many experiments demonstrated the significant impact of environmental factors on the degradation of the device. Niu *et al.* [19] identified the extrinsic factors causing the degradation of the perovskite film, such as moisture and oxygen, ultra violet (UV) light, and thermal effect. As suggested by Burschka *et al.* [7], in particular, $MAPbI_3$ can be degraded easily under humid condition, and therefore, the humidity should not be over 1% during the device fabrication. The series of reactions for the moisture catalyzed decomposition of $MAPbI_3$ into the by-products including PbI_2(s), CH_3NH_2(aq), I_2(s), H_2(g) and H_2O, which is irreversible, were proposed [8], and corroborated by measuring the X-ray diffraction (XRD) patterns before and after exposure to moisture [19, 22, 23], and the photothermal deflection spectroscopy [24]. Under illumination of UV light as well, the deterioration of PSC was occurred owing to not $MAPbI_3$ but TiO_2 scaffold, which is often used as transporting layer of conduction electrons. To explain this phenomena, the hypothesis was raised such that the electrons injected into TiO_2 layer might be trapped in deep lying unoccupied sites [25]. Thermal effect is also a considerable factor in the stability of compound. When elevating the environmental temperature, $MAPbI_3$ may be decomposed into PbI_2 and CH_3NH_3I (or subsequently CH_3NH_2 and HI), as confirmed by different kinds of experiments [26, 27]. The origin of thermal decomposition was likely to be structural defects. It was also observed

that the interface with TiO_2 or ZnO layer plays a role in the thermal decomposition, whose mechanism was suggested to be a deprotonation of the MA cation in contact with the interface [28].

In addition to such extrinsic factors, Zhang *et al.* [29] reported from first-principles calculations that $MAPbI_3$ is intrinsically instable. The authors calculated the energy change for the phase separation, $CH_3NH_3PbI_3 \rightarrow CH_3NH_3I + PbI_2$, showing that this reaction is exothermic and thus it may occur spontaneously even without any moisture, oxygen or UV light in the environment. Once it is formed, however, the kinetic barrier may prevent the compound from phase separation, so that $MAPbI_3$ may still be stable for a certain period to be used safely in PSCs. In addition, they suggested a promising method to improve the stability of PSCs, *i.e.,* substitution of ingredient ions by similar elements, e.g., replacing Pb^{2+} by Sn^{2+}, I^- by Br^- or Cl^-, or $CH_3NH_3^+$ by Cs^+. In this context, it is remarkable to tune the efficiency as well as operational stability of PSCs by adjusting the structural composition and order of mixed halide perovskite compounds [30–32].

The most favorable attempt to improve the material instability of $MAPbI_3$ is to replace I ions with Br or Cl ions [31, 33, 34]. Noh *et al.* [31] showed that increasing the Br content x in $MAPb(I_{1-x}Br_x)_3$ causes a phase transition, e.g., from tetragonal to cubic at x=0.13, and moreover altered the band gap following the quadratic function of Br content, $E_g(x) = 1.57 + 0.39x + 0.33x^2$ (eV). For low Br concentration (x<0.2), in particular, while the efficiency almost unchanged, the stability of device was found to be significantly improved. When exposing to a relative humidity of 55%, the cells underwent the significant degradation for the x=0 and x=0.06 cases, but for higher Br contents (x=0.2 and x=0.29) no large degradation was observed within the 20 days measurement period. It was suggested that the improved stability for higher Br content is due to a reduced lattice constant and a phase transition from tetragonal to cubic phase. In spite of such experiments, few theoretical study based on the first-principles method to uncover the fundamental mechanism of the stability improvement by substituting Br for I can be found, to the best of our knowledge.

In this work, we investigate the mixed iodide-bromide perovskite compounds $MAPb(I_{1-x}Br_x)_3$ to address the effects of Br substitution on the material properties at the electronic scale. To conduct the first-principles simulations of solid solutions with moderate computational cost, we utilize the virtual crystal approximation (VCA) [35, 36] rather than the supercell method. As increasing the Br content x from 0.0 to 1.0 with the interval of 0.1,

the lattice parameters and band gaps are calculated and compared with the experiments to verify the validity of the underlying VCA method. Furthermore, we describe a method to approximately calculate the exciton binding energy, and with this, demonstrate the merit of charge carrier generation and transportation in these materials. Finally, we find the most favorable Br content for material stability to be x=0.2 by performing an analysis of bonding characteristics.

II. METHOD

A. Exciton binding energy

To calculate the exciton binding energy, we make use of effective mass approximation, in which an exciton made up of a hole and an electron can be viewed as a hydrogen atom. Therefore, the Schrödinger equation for an excitonic system can be written as follows,

$$\left(-\frac{\hbar^2}{2m_h^*}\Delta_h - \frac{\hbar^2}{2m_e^*}\Delta_e - \frac{1}{4\pi\varepsilon\varepsilon_0}\cdot\frac{e^2}{|\boldsymbol{r}_h-\boldsymbol{r}_e|}\right)\psi_n(\boldsymbol{r}_h,\boldsymbol{r}_e) = E_n\psi_n(\boldsymbol{r}_h,\boldsymbol{r}_e) \tag{1}$$

where ε_0 is dielectric constant of vacuum. The difference between hydrogen atom and the excitonic system is attributed to the replacement of electron and nucleus masses with the effective masses of electron (m_e^*) and hole (m_h^*), and to the consideration of the dielectric constant ε of surrounding material in the Coulomb interaction. Dealing with Equation 1 in the same way of solving the Schrödinger equation for hydrogen atom gives the eigenvalues of excitonic system as follows,

$$E_n = -\frac{m_r^* e^4}{2\left(4\pi\varepsilon\varepsilon_0\right)^2\hbar^2}\cdot\frac{1}{n^2} = -\frac{m_e e^4}{2(4\pi\varepsilon_0)^2\hbar^2}\cdot\frac{m_r^*}{m_e}\cdot\frac{1}{\varepsilon^2}\cdot\frac{1}{n^2} \approx -13.56\cdot\frac{m_r^*}{m_e}\cdot\frac{1}{\varepsilon^2}\cdot\frac{1}{n^2}\ (\text{eV}) \tag{2}$$

where m_r^* is the reduced mass given from the effective masses of electron and hole as follows,

$$m_r^* = \frac{m_e^*\cdot m_h^*}{m_e^*+m_h^*} \tag{3}$$

Then, the exciton binding energy can be obtained by calculating the energy needed to send the effective electron in the energy level E_1 to the infinity E_∞ (ionization energy), i.e.,

$$E_b = -(E_\infty - E_1) \approx 13.56\cdot\frac{m_r^*}{m_e}\cdot\frac{1}{\varepsilon^2}\ (\text{eV}) \tag{4}$$

Therefore, to calculate the exciton binding energy with this method, we need to know the static dielectric constant of materials and the effective masses of electron and hole, which can be obtained readily through the first-principles calculations.

B. Computational method

For all relevant atoms, the optimized norm-conserving pseudopotentials with the designed nonlocal potential suggested by Rappe *et al.* [37] were constructed using the Opium package [49]. The valence electronic configurations of atoms are as follows; H–$1s^1$, C–$2s^2 2p^2$, N–$2s^2 2p^3$, Br–$4s^2 4p^5$, I–$5s^2 5p^5$, and Pb–$5d^{10} 6s^2 6p^2$. Here, the pair of Br and I atoms, having the same valence electronic configuration, was treated as the virtual atom. To construct the pseudopotential of this virtual atom, we have utilized the *Yu-Emmerich extended averaging approach* (YE^2A^2 in short) [35], in which both potentials and wavefunctions are averaged. The Perdew-Burke-Ernzerhof (PBE) [38] formalism for exchange-correlation functional within generalized gradient approximation (GGA) was used to generate the pseudopotentials and further perform the crystalline solid simulations.

The crystalline structure of $MAPb(I_{1-x}Br_x)_3$ was assumed to be pseudo-cubic with a space group of Pm as confirmed by XRD measurement [39]. As shown in Figure 1, the MA cation is oriented to the (101) direction, which is regarded as the lowest energetic configuration among the different orientations [11].

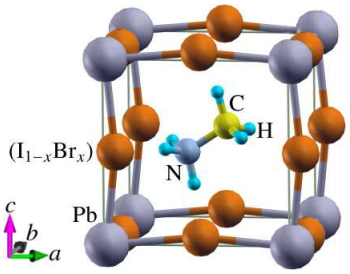

FIG. 1: (Color online) Ball-and-stick model of unit cell of $CH_3NH_3Pb(I_{1-x}Br_x)_3$ compound with pseudo-cubic crystalline lattice and $CH_3NH_3^+$ cation oriented to (101) direction.

In this work, we have used the pseudopotential plane-wave method as implemented in the ABINIT (version 7.10.2) package [40, 41]. The plane wave cut-off energy was set to be 40 Ha and k-points mesh to be (4×4×4) for structural optimization, which guarantee the total energy convergence to be 5 meV per unit cell. For the calculations of frequency dependent dielectric constants, electronic band structure and density of states (DOS), denser k-point meshes (12×12×12) were used. To determine the optimized crystalline structure, we have calculated the total energies of the crystalline unit cells as varying the volumes evenly,

at which all the atomic positions were relaxed until the atomic forces reached 0.01eVÅ^{-1}. Then, the optimized lattice constant was determined by fitting the $E-V$ data into the Birch-Murnaghan equation of state.

Using the optimized unit cells, the frequency dependent dielectric constants, $\varepsilon(\omega)$=$\varepsilon_1(\omega)$+$i\varepsilon_2(\omega)$, were calculated within the density functional perturbation theory (DFPT) [42]. Then, the photoabsorption coefficients as a function of frequency ω can be obtained using the following equation,

$$\alpha(\omega) = \frac{2\omega}{c}\sqrt{\frac{1}{2}\left(-\varepsilon_1(\omega) + \sqrt{\varepsilon_1^2(\omega) + \varepsilon_2^2(\omega)}\right)} \tag{5}$$

Note that the electron-hole coupling was not considered in this work, due to quite a heavy computational cost in the scheme based on the Bethe-Salpeter equation for the two-body Green's function. However, it was known that in the case of small band gap materials ignoring electron-hole coupling still leads to quite reasonable spectra compared to experiment.

III. RESULTS AND DISCUSSION

We first determined the lattice constants of the pseudo-cubic crystals by estimating the $E-V$ data and then fitting it into the Birch-Murnaghan equation of state. Here, the $E-V$ data was obtained by calculating the total energies of atomic-relaxed unit cells at fixed volume, as increasing the volume gradually from $0.9V_0$ to $1.1V_0$, where V_0 is the volume of optimized unit cell. This process was repeated at each Br content x, which was varied from 0 to 1 with the interval of 0.1.

In Figure 2, we show the optimized lattice constants as a function of Br content x in $MAPb(I_{1-x}Br_x)_3$ compounds. With the increase of the Br content, the lattice constants of the pseudo-cubic crystalline phases decrease due to the partial substitution of the larger iodine ion (ionic radius 2.2 Å) with the smaller bromine ion (ionic radius 1.96 Å). It is well-known that the mixed perovskites composed of two different perovskite crystals with similar lattices are expected to follow the Vegard's law, which indicates the linear dependence of lattice constants on the compositional variation. To illustrate the satisfaction of Vegard's law in the mixed halide perovskites, we have performed the interpolation of the calculated lattice constants as a linear function of Br content x, resulting in the formula, $a(x) = 6.420-0.333x$ (Å), which is comparable to the fitting line $a(x) = 6.325 - 0.384x$ (Å) to the experimental

data [43]. Although the linear coefficient in the fitting line to the computational data is in good agreement with that to the experiment, the lattice constant at $x = 0$ was overestimated the experiment with a relative error of 1.5% and thus the line was over-shifted in y-axis with the same magnitude. We attribute this to the PBE-GGA exchange-correlation functional, which is in general expected to give overestimation of lattice parameters. Despite such deviation in the magnitude of lattice constants, the tangents were almost identical each other, indicating the satisfaction of Vegard's law, so that we can use our VCA method safely to draw a meaningful conclusion in the following.

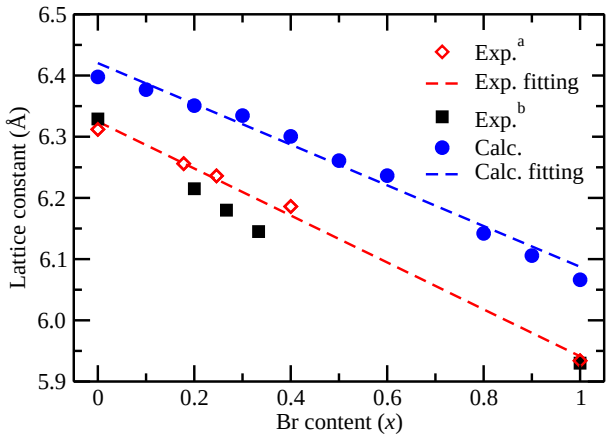

FIG. 2: (Color online) Lattice constants as a function of Br content x in the mixed halide perovskites $CH_3NH_3Pb(I_{1-x}Br_x)_3$, with linear fitting lines (dashed lines). Red diamonds indicate the experimental values in Ref. [43], filled black squares in Ref. [34], and filled blue circles mean the calculated values in this work.

We then investigated the variation tendency in electronic structures as increasing the Br content in the mixed $MAPb(I_{1-x}Br_x)_3$ perovskites, doing this with the energy band structures and partial density of states (DOS) projected on each atom. The calculated band-gaps and DOSs as functions of Br content x are shown in Figure 3. We should note that the electronic band structures and DOSs are gradually changed without any anomaly as the Br content is varied, again showing the reliability of the VCA method.

We shed light on that the band gaps are in direct mode at R point in reciprocal space over all the Br contents, shown in Figure 3 (a). This is one of the most advantageous aspects of the mixed halide perovskites $MAPbX_3$, so that the exciton (electron-hole pair) can be generated directly by light absorption without any other process like phonon. On the contrary to the

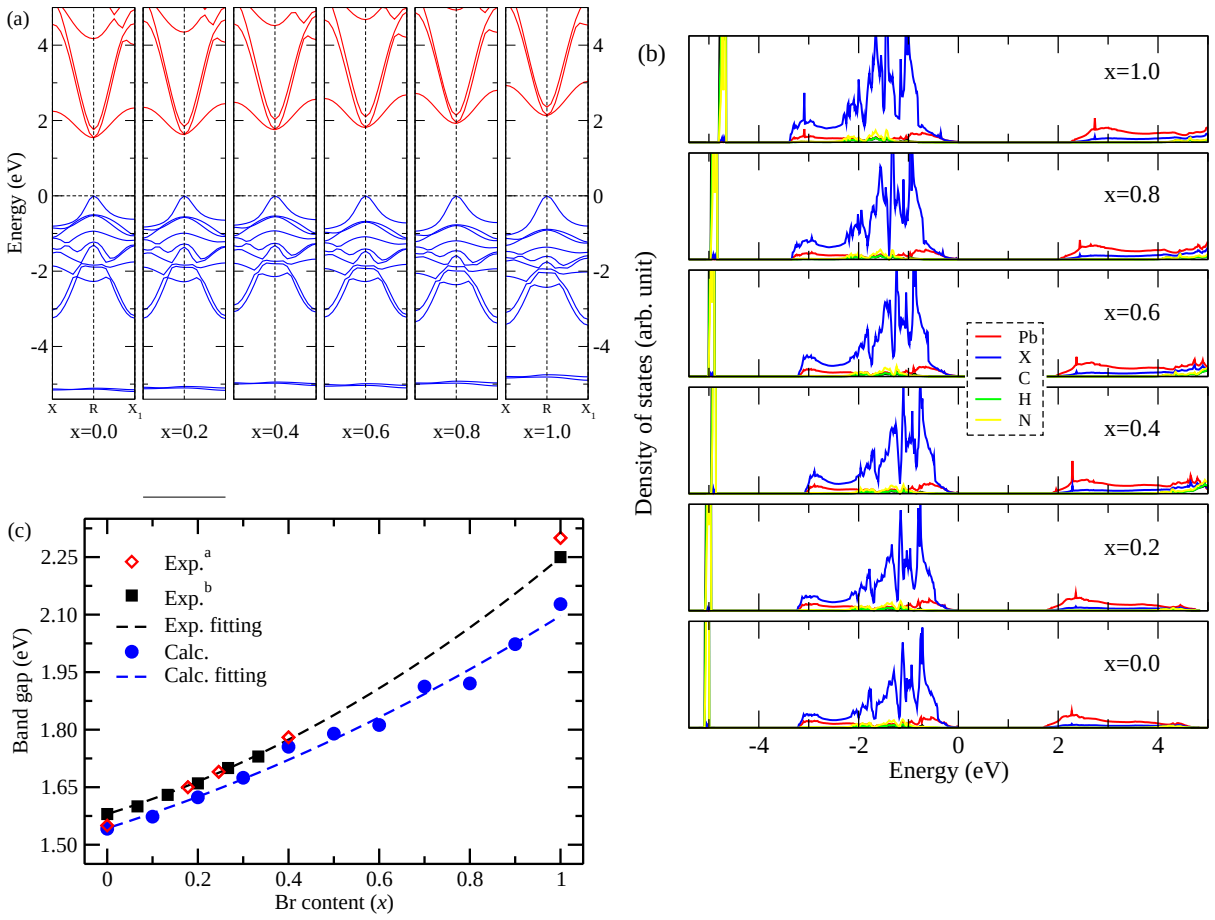

FIG. 3: (Color online) Electronic structures of $CH_3NH_3Pb(I_{1-x}Br_x)_3$ with the variation of Br content x, as calculated by VCA method within DFT. (a) Electronic energy band structures around R point, (b) atomic resolved density of states, setting the top of valence band to be zero, and (c) energy band gaps as quadratic functions of Br content x. A virtual atom ($I_{1-x}Br_x$) is denoted X in (b). Exp.^{a} and Exp.^{b} data in (c) are from Ref. [43] and Ref. [34], respectively.

case of lattice constants, the band gaps were slightly underestimated the experimental values, going further underestimation from $MAPbI_3$ ($x = 0$) to $MAPbBr_3$ ($x = 1$). Nevertheless, the deviations of band gaps from the experimental values, e.g., 0.01 eV at $x = 0$ and 0.1 eV at $x = 1$, are thought to be not very large but rather reasonably good, compared to the PBE-GGA applications to the other semiconducting compounds (the deviation $\sim$ 1 eV in general). Such a good agreement in band-gaps of these organic-inorganic halide perovskites could be explained by a fortuitous cancellation of errors, namely, the GGA underestimation

is counterbalanced by the lack of spin-orbit interaction [44]. When occurring the substitution of heavier iodine atom ($Z = 53$) by lighter bromine atom ($Z = 35$), the effect of spin-orbit interaction becomes weaker, and therefore, more underestimation of band gap at $MAPbBr_3$ ($x = 1$) could be expected as shown in this work.

To describe the variation tendency of band gaps with respect to the Br content, we have also interpolated the band gaps to the quadratic function of Br content x in Figure 3 (c),

$$E_g(x) = E_g(0) + [E_g(1) - E_g(0) - b]x + bx^2, \tag{6}$$

where $E_g(0)$ and $E_g(1)$ are band gaps of $MAPbI_3$ (x=0) and $MAPbBr_3$ (x=1) respectively, and b is the so-called bowing parameter [34]. Our calculations gave the formula $E_g(x) = 1.542 + 0.374x + 0.185x^2$ (eV), *i.e.,* $E_g(0) = 1.542$ eV, $E_g(1) = 2.101$ eV and $b = 0.185$ eV, which are in good agreement with those from experiments $E_g(0) = 1.58$ (1.579) eV, $E_g(1) = 2.28$ (2.248) eV and $b = 0.33$ (0.306) eV in Ref. [31] (Ref. [34]). The bowing parameter b reflects the fluctuation degree in the crystal field and the nonlinear effect arising from the anisotropic nature of binding [34]. Therefore, the quite small b values both in our calculation and the experiments indicate the low compositional disorder and a good miscibility between $MAPbI_3$ and $MAPbBr_3$. It is clear that the substitution of larger iodine ion by smaller bromine ion leads to the enhancement of interaction between Pb and X atoms in corner-sharing PbX_6 octahedron, which play a major role in determining the band structure [10, 45], and thus the decrease of lattice constant, resulting in the increase of band gaps with the implication of worsening the light harvesting properties from $MAPbI_3$ to $MAPbBr_3$.

We have done the analysis of the atomic resolved (and partial) DOSs in detail to seek the electronic factors possibly responsible for the band gap variation. As shown in Figure 3 (b), it is established that the valence band maximum (VBM) of $MAPbX_3$ has strong X p and Pb s antibonding character, while the conduction band minimum (CBM) mainly originates from Pb p orbital with a small contribution of X s orbital. It can be thought that Br $4p$ states tend to hybridize more strongly with Pb s states than I $5p$ states, causing the down-shift of VBM and thus the increase of band gaps. At this point, it is worth noting that, although the highest occupied molecular orbitals (HOMO) of MA cation are found deep $\sim$ 5 eV below the VBM, having narrow features, there is an interaction between organic MA cation and the inorganic PbX_6 octahedra by possible hydrogen bonding between ammonium

group and X atom. It is also interesting to notice that, when increasing the Br content, the energy interval between the HOMO of MA cation and the bottom level of PbX_6 is getting close, providing an indication of becoming stronger MA-PbX_6 interaction.

In order to directly estimate the light harvesting capability of PSCs, we next describe the photoabsorption coefficients of these mixed halide perovskites with different Br contents, which can be obtained from Equation (5) using the real and imaginary parts of frequency dependent dielectric constants, calculated within DFPT [42]. In Figure 4, we present the photoabsorption coefficients to be functions of photon energy as increasing the Br content. At lower Br content, the mixed halide perovskites $MAPb(I_{1-x}Br_x)_3$ exhibit the extended absorption character over the whole visible light spectrum, which is an advantageous property for light harvesting. For higher Br contents, however, the absorption onset gradually shifts to the higher photon energy, i.e., to shorter wavelength light. Such blue-shift of the absorption onsets can be readily expected from the rise of band gaps in the mixed halide perovskites $MAPb(I_{1-x}Br_x)_3$ with the increase of Br content.

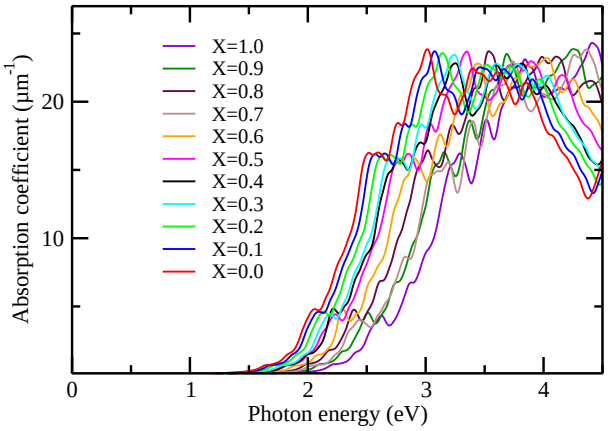

FIG. 4: (Color online) Photoabsorption coefficients of mixed halide perovskites $CH_3NH_3Pb(I_{1-x}Br_x)_3$ at different Br contents x, as calculated by VCA and DFPT method within DFT.

Another important properties to be unavoidably considered in the mixed halide perovskites are the binding energy between electron and hole, which are generated due to the photon absorption, and the mobility of these charge carriers. Of two properties, the exciton binding energy plays a key role in discriminating whether the charge carriers behave free particles as in normal inorganic thin-film semiconductors, or bound excitons as in organic

semiconductors. The weaker exciton binding energy indicates more freely behaving charge carriers. After the computation of the effective masses of electrons and holes by straightforward numerical process of the refined energy band data around R point in the first Brillouin zone, and the extraction of the static dielectric constants simply from the frequency dependent dielectric constants, we have used Equation (4) to calculate the exciton binding energy. The calculated data are listed in Table I.

TABLE I: Calculated effective masses of electron (m_e^*) and hole (m_h^*), static dielectric constant (ε), and exciton binding energy (E_b) of mixed halide perovskites $CH_3NH_3Pb(I_{1-x}Br_x)_3$ at the different Br contents x. The available experimental data are also presented.

				E_b (eV)	
x	m_h^*/m_e	m_e^*/m_e	ε	Calc.	Exp.
0.0	0.187	0.181	5.261	0.045	0.045[a]
0.1	0.189	0.183	5.098	0.049	-
0.2	0.204	0.192	4.946	0.055	-
0.3	0.224	0.212	4.733	0.066	-
0.4	0.228	0.221	4.634	0.071	-
0.5	0.230	0.224	4.599	0.073	-
0.6	0.238	0.228	4.380	0.082	-
0.7	0.241	0.213	4.189	0.087	-
0.8	0.229	0.206	4.028	0.091	-
0.9	0.231	0.210	3.929	0.097	-
1.0	0.241	0.197	3.862	0.099	0.088[b]

[a] Ref. [46]

[b] Ref. [47]

In spite of the rough approximation adopted in this work, the calculated exciton binding energies are in excellent agreement with the available experimental values, indicating the reliability of hydrogen-like model to these materials. On the basis of these data, we can say that the exciton binding energy increases in proportion to the Br content x in $MAPb(I_{1-x}Br_x)_3$, as the approximate formula $E_b(x) = 0.045 + 0.057x$ (eV). For low Br content, in particular, the exciton binding energies are quite small, being comparable to those of the inorganic thin-film semiconductors (< 50 meV), and therefore, the charge carriers are likely to behave

free-like. Meanwhile, those are large for higher Br contents, indicating that, when increasing the Br content, the excitons become to be bound. Note that the calculated static dielectric constants are in good agreement with the recent theoretical values calculated by quantum molecular dynamics method [12].

Then, let us see the effective masses of carriers, indirect estimation for the mobility of carriers. Despite some slight fluctuations from x=0.7 to x=1.0, it can be said that the effective masses of carriers also tend to increase when rising the Br content, and as a consequence, the mobility decreases conversely. To sum up the arguments so far, we can conclude that the substitution of iodine atom by bromine atom in mixed halide lead perovskites causes a little loss of advantageous properties of $MAPbI_3$ towards PSC application in overall. Then, what about the material stability?

To make an answer to this question, we pay our attention to the bonding characteristics in these mixed halide perovskites. In this work, we have focused on the variation tendency in the bond lengths between Pb and the virtual X ($I_{1-x}Br_x$) atoms, and in those between C and N atoms, at different Br contents from x=0.0 to x=0.5. In Table II, we summarize the bond lengths from our calculation with some available experimental values.

TABLE II: Calculated bond lengths between Pb and virtual X ($I_{1-x}Br_x$) atoms, and between C and N atoms, in the mixed halide perovskites $CH_3NH_3PbX_3$ at different Br contents. Some experimental values are also listed.

	$d_{\text{Pb-X}}$ (Å)		$d_{\text{C-N}}$ (Å)	
x	Calc.	Exp.[a]	Calc.	Exp.[a]
0.0	3.3227	3.16	1.4880	1.48
0.1	3.3172		1.4872	
0.2	3.3024		1.4880	
0.3	3.3099		1.4877	
0.4	3.3069		1.4876	
0.5	3.2911		1.4874	

[a] Ref. [48]

It is worth to note that the calculated C-N bond length at x=0 is in good agreement with the experimental value, while the calculated Pb-I bond length is overestimated compared to the experiment due to the overestimation of lattice constant. To see the variation tendency

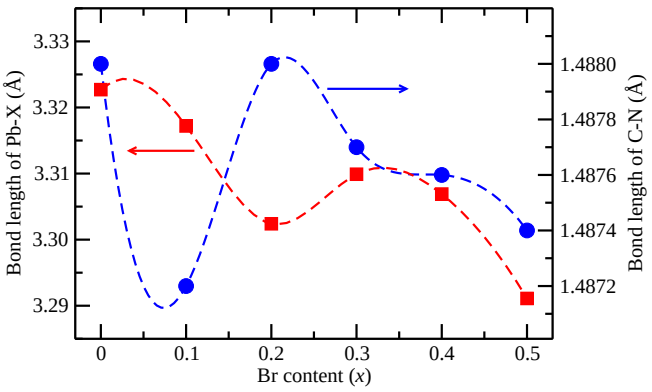

FIG. 5: (Color online) Curves of bond lengths between Pb and virtual X ($I_{1-x}Br_x$) atoms, and between C and N atoms in the mixed halide perovskites $CH_3NH_3PbX_3$ with different Br content x.

more intuitively, we also plot the variation curves of bond lengths as functions of Br content in Figure 5. Most interestingly, the Pb-X bond length is in local minimum, whereas C-N bond length is in maximum, at x=0.2 in the range from x=0.0 to x=0.5. In fact, it would be expected that, since the lattice constant decreases with the increase of the Br content, the Pb-X bond length also would tend to decrease in the same mode. However, the observations were over our expectation. This indicates that at x=0.2 the Pb-X bond has the strongest coupling and the MA cation compacts the PbX_6 octahedra, resulting in a potential improvement of material stability. Our computational results exactly coincide with the experimental findings that the efficiency remains quite stable at x=0.2 and x=0.29, being lower efficiency in the latter case, whilst severe decrease of efficiency at x=0.0 and x=0.06 [20, 31]. Since the efficiency is expected not to be much spoiled at x=0.2 with the lattice constant of 6.352 Å, the band gap of 1.624 eV and the exciton binding energy of 0.055 eV, it can be suggested that the best match between efficiency and stability can be realized at x=0.2 in the mixed halide perovskites $MAPb(I_{1-x}Br_x)_3$.

To assist in uncovering how the best match can be achieved at x=0.2, we have made a comparison between the calculated atomic orbitals corresponding to the VBM at R point with the different Br contents (x=0.0, 0.1, 0.2, 0.3). In Figure 6, the Pb s-type orbitals are shown at x=0.0, 0.1 and 0.3, which are agreed with the above discussion of DOSs, but at x=0.2 the Pb p-type orbital is observed to our surprise. This indicates that the VBM comes from the $s-p$ hybridization between the Pb s and X p orbitals, except at x=0.2

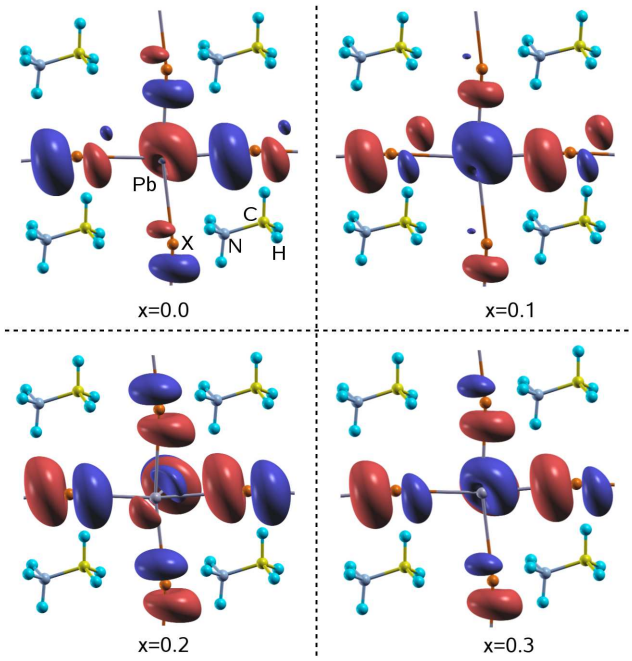

FIG. 6: (Color online) Isosurface plots of atomic orbitals corresponding to the VBM at R point with different Br contents (x=0.0, 0.1, 0.2, 0.3) in the mixed halide perovskites $CH_3NH_3Pb(I_{1-x}Br_x)_3$, as calculated by VCA method within DFT. The isosurface is evaluated at $\pm 1.3/\sqrt{\Omega}$, being Ω the unit-cell volume.

where the strong σ bonding between Pb p and X p-type orbitals is occurred. Since it can be thought that the σ bonding strengthens the Pb-X binding, the stability enhancement can be expected at x=0.2 in the mixed halide perovskites $MAPb(I_{1-x}Br_x)_3$. We regard this work will contribute to the fundamental understanding of material properties of mixed halide perovskites $MAPb(I_{1-x}Br_x)_3$ with an offer of useful guide to tune their efficiency and stability by adjusting the Br content.

IV. CONCLUSION

Despite the remarkable advances in the performance of hybrid halide perovskites, yet the degradation and instability in these materials remain barrier to the practical use in solar cell applications. In this work, using the VCA method within DFT, we have investigated the influence of halide composition on the structural, electronic, and optical properties of the mixed halide perovskites $MAPb(I_{1-x}Br_x)_3$. When increasing the Br content x from 0.0

to 1.0, we have found the decrease of lattice constants with the linear function of $a(x) = 6.420 - 0.333x$ (Å), while the increase of band gaps and exciton binding energies with the quadratic function of $E_g(x) = 1.542 + 0.374x + 0.185x^2$ (eV) and the linear function of $E_b(x) = 0.045 + 0.057x$ (eV) respectively. The increase of band gaps with the Br content is due to the stronger hybridization of Br $4p$ states with Pb s states than I $5p$ states, which leads to the down-shift of VBM, together with the decrease of lattice constant. With the increase of the Br content, the energy interval between the HOMO of MA cation and the bottom level of PbX_6 is getting close, providing an indication of becoming stronger MA-PbX_6 interaction. The calculated photoabsorption coefficients exhibit the blue-shift of absorption onsets for higher Br content. The substitution of I atom by Br atom leads to the enhancement of stability, which is described by analysing the bonding characteristics. In conclusion, our work suggests that, considering the tunability of material properties by adjusting the Br content x in the mixed halide perovskites $MAPb(I_{1-x}Br_x)_3$, the best match between efficiency and stability might be achieved at x=0.2.

Acknowledgments

This work was supported partially from the Committee of Education, Democratic People's Republic of Korea, under the project entitled "Strong correlation phenomena at superhard, superconducting and nano materials" (grant number 02-2014). The simulations have been carried out on the HP Blade System c7000 (HP BL460c) that is owned and managed by the Faculty of Materials Science, Kim Il Sung University.

---

[1] H. Zhou, Q. Chen, G. Li, S. Luo, T.-B. Song, H.-S. Duan, Z. Hong, J. You, Y. Liu, and Y. Yang, Science **345**, 542 (2014).

[2] N. J. Jeon, J. H. Noh, W. S. Yang, Y. C. Kim, S. Ryu, J. Seo, and S. I. Seok, Nature **517**, 476 (2015).

[3] J. Liu, J. Lin, Q. Xue, Q. Ye, X. He, L. Ouyang, D. Zhuang, C. Liao, H. L. Yip, J. Mei, et al., J. Power Sources **301**, 242 (2016).

[4] M. Liu, M. B. Johnston, and H. J. Snaith, Nature **501**, 395 (2013).

[5] S. Casaluci, L. Cinà, A. Pockett, P. S. Kubiak, R. G. Niemann, A. Reale, A. D. Carlo, and P. J. Cameron, J. Power Sources **297**, 504 (2015).

[6] F. D. Giacomo, S. Razza, F. Matteocci, A. D'Epifanio, S. Licoccia, T. M. Brown, and A. D. Carlo, J. Power Sources **251**, 152 (2014).

[7] J. Burschka, N. Pellet, S. J. Moon, R. Humphry-Baker, P. Gao, M. K. Nazeeruddin, and M. Grätzel, Nature **499**, 316 (2013).

[8] J. M. Frost, K. T. Butler, F. Brivio, C. H. Hendon, M. van Schilfgaarde, and A. Walsh, Nano Lett. **14**, 2584 (2014).

[9] R. Lindblad, D. Bi, B. w. Park, J. Oscarsson, M. Gorgoi, H. Siegbahn, M. Odelius, E. M. J. Johansson, and H. Rensmo, J. Phys. Chem. Lett. **5**, 648 (2014).

[10] J. Even, L. Pedesseau, J.-M. Jancu, and C. Katan, J. Phys. Chem. Lett. **4**, 2999 (2013).

[11] F. Brivio, A. B. Walker, and A. Walsh, APL Matter **1**, 042111 (2013).

[12] T. Hakamata, K. S. abd F. Shimojo, R. K. Kalia, A. Nakano, and P. Vashishta, Sci. Rep. **6**, 19599 (2016).

[13] S. D. Stranks and H. J. Snaith, Nat. Nanotechnol. **10**, 391 (2015).

[14] E. Edri, S. Kirmayer, S. Mukhopadhyay, K. Gartsman, G. Hodes, and D. Cahen, Nat. Commun. **5**, 3461 (2014).

[15] Q. Lin, A. Armin, R. C. R. Nagiri, P. L. Burn, and P. Meredith, Nat. Photonics **9**, 106 (2014).

[16] J. S. Manser and P. V. Kamat, Nat. Photonics **8**, 737 (2014).

[17] Y. Yamada, T. Nakamura, M. Endo, A. Wakamiya, and Y. Kanemitsu, J. Am. Chem. Soc. **136**, 11610 (2014).

[18] S. D. Stranks, G. E. Eperon, G. Grancini, C. Menelaou, M. J. P. Alcocer, T. Leijtens, L. M. Herz, A. Petrozza, and H. J. Snaith, Science **342**, 341 (2013).

[19] G. Niu, X. Guo, and L. Wang, J. Mater. Chem. A **3**, 8970 (2015).

[20] D. Wang, M. Wright, N. K. Elumalai, and A. Uddin, Sol. Energy Mater. Sol. Cells **147**, 255 (2016).

[21] Z. Xiao, Y. Yuan, Q. Wang, Y. Shao, Y. Bai, Y. Deng, Q. Dong, M. Hu, C. Bi, and J. Huang, Mater. Sci. Eng. R **101**, 1 (2016).

[22] J. Yang, B. D. Siempelkamp, D. Liu, and T. L. Kelly, ACS Nano **9**, 1955 (2015).

[23] J. A. Christians, P. A. M. Herrera, and P. Kamat, J. Am. Chem. Soc. **137**, 1530 (2015).

[24] S. D. Wolf, J. Holovsky, S. J. Moon, P. Loper, B. Niesen, M. Ledinsky, F. J. Haug, J. H. Yum,

and C. Ballif, J. Phys. Chem. Lett. **5**, 1035 (2014).

[25] T. Leijtens, G. E. Eperon, S. Pathak, A. Abate, M. M. Lee, and H. J. Snaith, Nat. Commun. **4**, 2885 (2013).

[26] A. Dualeh, P. Gao, S. I. Seok, M. K. Nazeeruddin, and M. Grätzel, Chem. Mater. **26**, 6160 (2014).

[27] B. Conings, J. Drijkoningen, N. Gauquelin, A. Babayigit, J. D'Haen, L. D'Olieslaeger, A. Ethirajan, J. Verbeeck, J. Manca, E. Mosconi, et al., Adv. Energy Mater. **5**, 1500477 (2015).

[28] J. Yang, B. D. Siempelkamp, E. Mosconi, F. D. Angelis, and T. L. Kelly, Chem. Mater. **27**, 4229 (2015).

[29] Y.-Y. Zhang, S. Chen, P. Xu, H. Xiang, X.-G. Gong, A. Walsh, and S.-H. Wei, arXiv:1506.01301 (2015).

[30] E. Mosconi, A. Amat, M. K. Nazeeruddin, M. Grätzel, and F. D. Angelis, **117**, 13902 (2013).

[31] J. H. Noh, S. H. Im, J. H. Heo, T. N. Mandal, and S. I. Seok, Nano Lett. **13**, 1764 (2013).

[32] S. Aharon, B. E. Cohen, and L. Etgar, J. Phys. Chem. C **118**, 17160 (2014).

[33] A. Sadhanala, F. Deschler, T. H. Thomas, S. E. Dutton, K. C. Goedel, F. C. Hanusch, M. L. Lai, U. Steiner, T. Bein, P. Docampo, et al., J. Phys. Chem. Lett. **5**, 2501 (2014).

[34] L. Atourki, E. Vega, B. Marì, M. Mollarb, H. A. Ahsainec, K. Bouabida, and A. Ihlal, Appl. Surf. Sci. **371**, 112 (2016).

[35] C.-J. Yu and H. Emmerich, J. Phys.: Condens. Matter **19**, 306203 (2007).

[36] J. Iniguez, D. Vanderbilt, and L. Bellaiche, Phys. Rev. B **67**, 224107 (2003).

[37] A. M. Rappe, K. M. Rabe, E. Kaxiras, and J. D. Joannopoulos, Phys. Rev. B **41**, 1227 (1990).

[38] J. P. Perdew, K. Burke, and M. Ernzerhof, Phys. Rev. Lett. **77**, 3865 (1996).

[39] T. Baikie, Y. Fang, J. M. Kadro, M. Schreyer, F. Wei, S. G. Mhaisalkar, M. Grätzel, and T. J. White, J. Mater. Chem. A **1**, 5628 (2013).

[40] X. Gonze, B. Amadon and P. M. Anglade *et al.*, Comput. Phys. Commun. **180**, 2582 (2009).

[41] X. Gonze, G.-M. Rignanese and M. Verstraete *et al.*, Z. Kristallogr. **220**, 558 (2005).

[42] S. Sharma, J. K. Dewhurst, and C. Ambrosch-Draxl, Phys. Rev. B **67**, 165332 (2003).

[43] R. K. Misra, L. Ciammaruchi, S. Aharon, D. Mogilyansky, L. Etgar, I. Visoly-Fisher, and E. A. Katz, arXiv:1603.08683 (2016).

[44] C. Motta, F. El-Mellouhi, S. Kais, N. Tabet, F. Alharbi, and S. Sanvito, Nature Commun. **6**, 7026 (2015).

[45] M. A. Green, A. Ho-Baillie, and H. J. Snaith, Nat. Photonics **8**, 506 (2014).

[46] T. C. Sum and N. Mathews, Energy Environ. Sci. **7**, 2518 (2014).

[47] D. Moses, J. Wang, A. Heeger, N. Kirova, and S. Brazovski, Proc. Natl. Acad. Sci. **98**, 13496 (2001).

[48] C. C. Stoumpos, C. D. Malliakas, and M. G. Kanatzidis, Inorg. Chem. **52**, 9019 (2013).

[49] The Opium package has features of atomic structure calculation, norm-conserving pseudopotential generation, and conversion into the fhi format, which is acceptable to the ABINIT package, being available at http://opium.sourceforge.net.